Supplementary Material

UiO-66-NH_2 @ benzotrithiophene-based COF composites with core-shell structure for effective adsorption of dyes

Xinhong Zhao[1], Rong Ma[1], Yuanyuan Li[*], Yulong Ma, Wenxin Ji, Yonggang Sun

*State Key Laboratory of High-efficiency Utilization of Coal and Green Chemical Engineering, College of Chemistry and Chemical Engineering, Ningxia University, Yinchuan 750021, P. R. China**

*** Correspondence should be addressed to Yuanyuan Li at the following address.**

(*State Key Laboratory of High-efficiency Utilization of Coal and Green Chemical Engineering, College of Chemistry & Chemical Engineering, Ningxia University*)

E-mail:liyuanyuan_abc@sohu.com

Materials and Reagents

All chemicals and reagents used in this study were of analytical grade or higher and were used without further purification. Zirconium chloride, N, N-dimethylformamide (DMF), acetic acid, methanol, 1,4-dioxane, I_2, RB, and tetrahydrofuran (THF) were all purchased from Aladdin (Shanghai, China). 2-aminoterephthalic acid and TC were purchased from Macklin Inc. (Shanghai, China). Benzidine (BZ) was obtained from Len Technology Co., Ltd. (Shanghai, China). p-Phenylenediamine (PD) and naphthalene-1,4-diamine (NPDA) were supplied by Bide Pharmatech Ltd. (Shanghai, China). CR was sourced from Beilian Fine Chemicals Development Co., Ltd. (Shanghai, China). MO and MB were procured from Beijing Chemical Works (China). MG was acquired from Sinopharm Chemical Reagent Co., Ltd. (Shanghai, China). Crystal Violet (CV) was provided by Zhongqin Chemical Reagent Co., Ltd. (Shanghai, China).

Experimental Instruments and Characterization

Functional group information was obtained through Fourier Transform Infrared Spectroscopy (FT-IR, Spectrum Two, PerkinElmer), with scan data recorded in the 400–4000 cm^{-1} range. X-ray Diffraction (XRD, D8 ADVANCE A25, Bruker AXS GmbH, Germany) was employed to characterize the samples' crystallinity and crystal structure. A fully automated BET-ASAP 2460 (Micromeritics) was employed for N_2 adsorption-desorption analysis based on the Brunauer-Emmett-Teller (BET) and Barrett-Joyner-Haldane (BJH) models to calculate the specific surface area and pore size distribution of the material. Surface morphology and internal pore structure were observed using a cold field emission scanning electron microscope (SEM, Regulus 8100, Hitachi Ltd.) at an acceleration voltage of 15.00 kV. Shell thickness and uniformity were examined via a field emission transmission electron microscope (TEM, Talos 200S, FEI Company). Chemical composition and surface chemical states were measured using X-ray photoelectron spectroscopy (XPS, AXIS SUPRA, Shimadzu Corporation). The absorbance of the three dye aqueous solutions before and after adsorption was determined using a UV spectrophotometer (UV-3300, Shanghai Meipu Instrument Co., Ltd.), and their concentrations were obtained by plotting standard curves.

Batch Adsorption Experiment

A typical adsorption experiment was conducted as follows: 20 mg of an adsorbent (UiO-66-NH_2@COF1, UiO-66-NH_2@COF2, UiO-66-NH_2@COF3, COF1-BTT-BZ, COF2-BTT-PD, COF3-BTT-NPDA, or UiO-66-NH_2) was added to a conical flask containing 40 mL of a 1000 mg/L dye solution (CR, RB, or MG). The mixture was first sonicated for 5 minutes and then transferred to a mechanical shaker for oscillation at 298 K for 2 hours. Afterwards, the solution was allowed to stand for approximately 1 hour to achieve solid-liquid separation. Finally, the residual concentrations of CR, RB, and MG in the supernatant were determined using a UV-Vis spectrophotometer at their respective characteristic wavelengths of 498 nm, 554 nm, and 617 nm.

Calculate adsorption capacity based on the adsorption equation:

$$q_t = \frac{(C_0 - C_t) * V}{m} \quad (1)$$

$$q_e = \frac{(C_0 - C_e) * V}{m} \quad (2)$$

In the above formula, q_t (mg/g) and q_e (mg/g) represent the adsorption capacity at time t and the adsorption capacity at equilibrium, respectively. C_0 (mg/L) represents the initial concentration of the three dyes, C_t (mg/L) represents the concentration after adsorption time t, C_e (mg/L) represents the concentration after adsorption reaches equilibrium, V (L) represents the volume of the solution, and m (g) represents the mass of the adsorbent.

Adsorption isotherms

Batch adsorption experiments investigated the effects of adsorption time, initial concentration, adsorption temperature, and initial solution pH on the adsorption capacities of CR, RB, and MG. To obtain adsorption isotherms, tests were conducted at different initial concentrations for each pollutant. In the experiments, the adsorption isotherms were fitted using the Langmuir and Freundlich models. The formula corresponding to the Langmuir model is expressed as follows:

$$q_e = \frac{q_{max} * K_L * C_e}{1 + K_L * C_e} \quad (3)$$

Its linearized form:

$$\frac{C_e}{q_e} = \frac{1}{K_L * q_{max}} + \frac{C_e}{q_{max}} \quad (4)$$

The formula corresponding to the Freundlich model is expressed as follows:

$$q_e = K_F * C_e^{1/n} \quad (5)$$

Its linearized form:

$$Lnq_e = LnK_F + \frac{1}{n} LnC_e \quad (6)$$

In the above formulas, q_{max} (mg/g) represents the maximum monolayer adsorption capacity, K_L (L/mg) represents the Langmuir adsorption equilibrium constant, K_F ((mg/g)(L/mg)$^{1/n}$ represents the Freundlich adsorption capacity constant, and n represents the dimensionless adsorption intensity constant.

Adsorption kinetics

To investigate adsorption kinetics, the residual concentrations of the three dyes were measured after adsorption for 10, 20, 30, 40, 50, 60, 120, and 240 minutes. To explore the adsorption mechanism, multiple kinetic models were employed to analyze the adsorption process, including pseudo-first-order kinetics, pseudo-second-order kinetics, and intra-particle diffusion models. The corresponding equations are expressed as follows:

$$Log_{(q_e - q_t)} = Log q_e - \frac{k_1 * t}{2.303} \quad (7)$$

$$\frac{t}{q_t} = \frac{1}{k_2 * q_e^2} \quad (8)$$

$$q_t = K_i \sqrt{t} + I \quad (9)$$

In the above formulas, k_1 (min^{-1}) represents the pseudo-first-order kinetic constant, and k_2 (g/(mg· min)) represents the pseudo-second-order kinetic constant. K_i ($mg/(g \cdot min^{1/2})$) is the intraparticle diffusion rate constant, and I (mg/g) is related to the boundary layer thickness.

Adsorption thermodynamics

The effect of ambient temperature on adsorption was investigated through experiments conducted at three distinct temperatures (298K, 308K, 318K). The corresponding thermodynamic equations are as follows:

$$\Delta G = \Delta H - T * \Delta S \quad (9)$$

$$Ln_k = -\frac{\Delta H}{RT} + \frac{\Delta S}{R} \quad (10)$$

The initial solution pH was adjusted using 0.1 M hydrochloric acid and 0.1 M sodium hydroxide to maintain the dye pH between 2 and 12. The effect of initial solution pH on adsorption capacity was investigated.

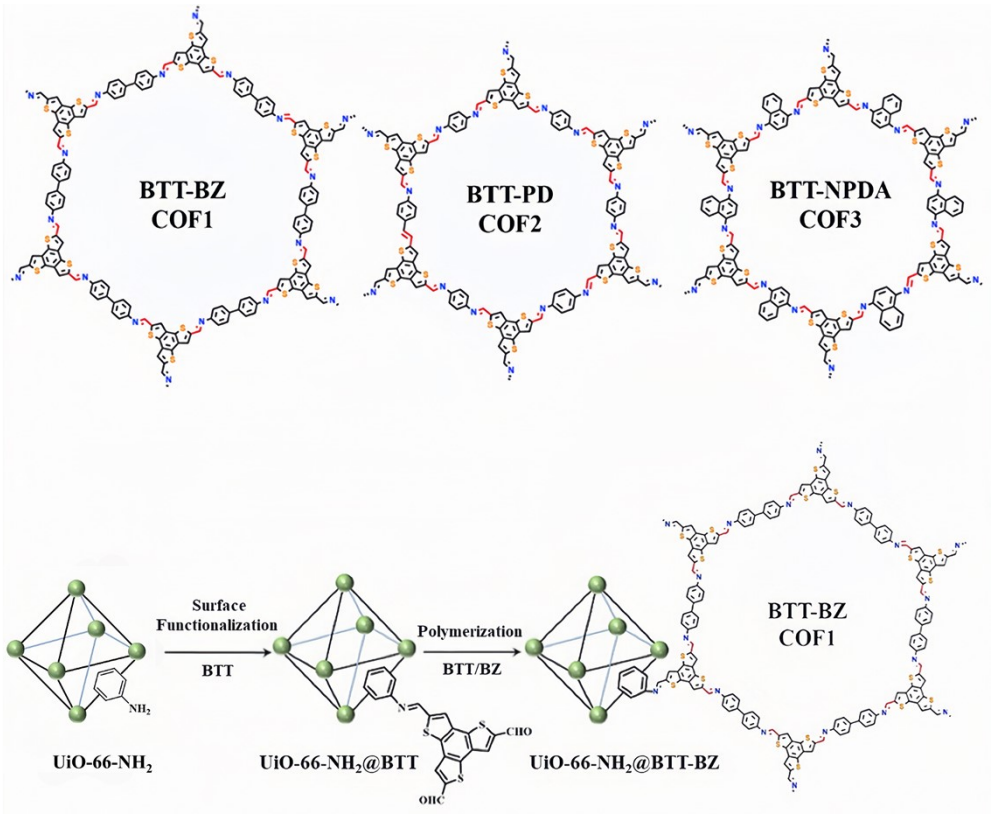

Fig S1 Structures of three COF materials and schematic diagram of the synthesis of UiO-66-NH_2@BTT-BZ.

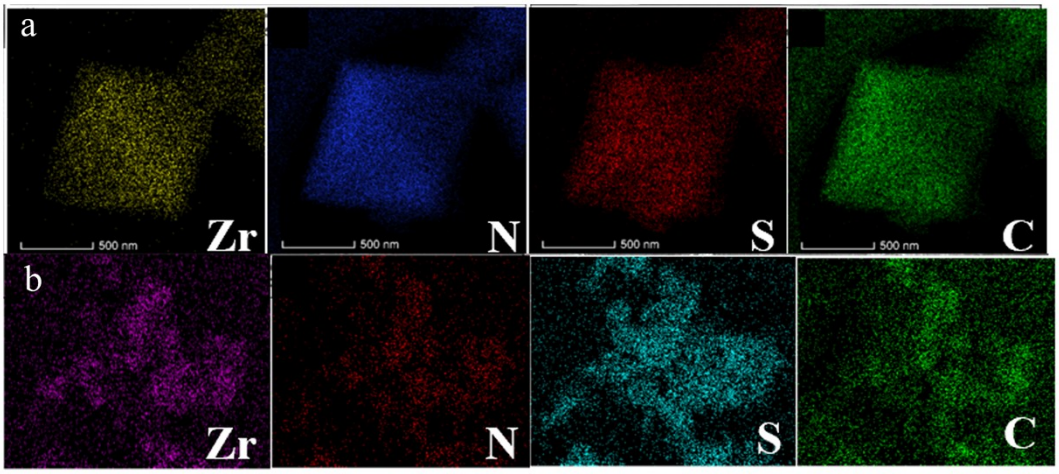

Fig S2. (a) (b) elemental mapping analysis on UiO-66-NH_2@COF1 and UiO-66-NH_2@COF2

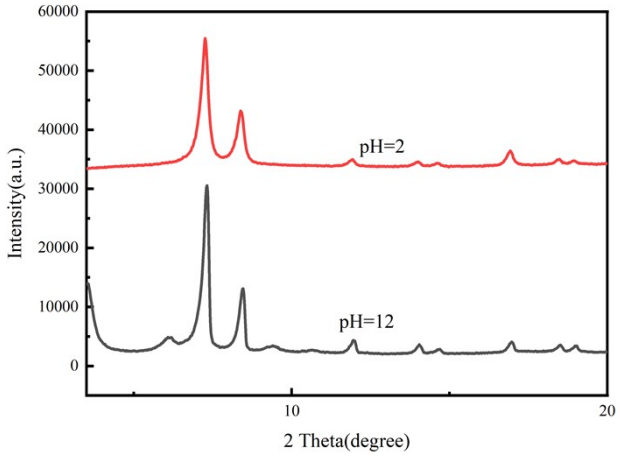

Fig S3. The XRD spectra of UiO-66-NH2@COF1 after adsorption under pH values of 2 and 12

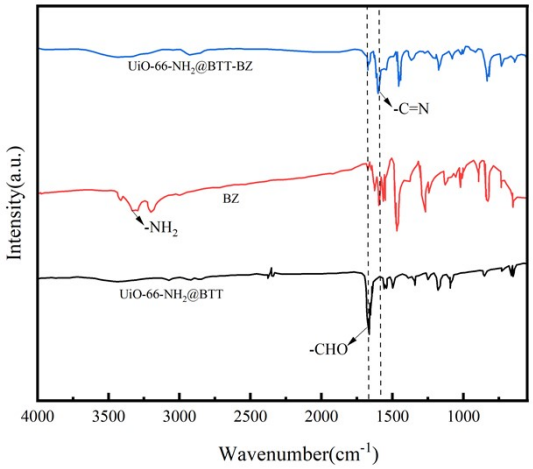

Fig S4. FT-IR spectra of UiO-66-NH_2@BTT, BZ, and UiO-66-NH_2@BTT-BZ

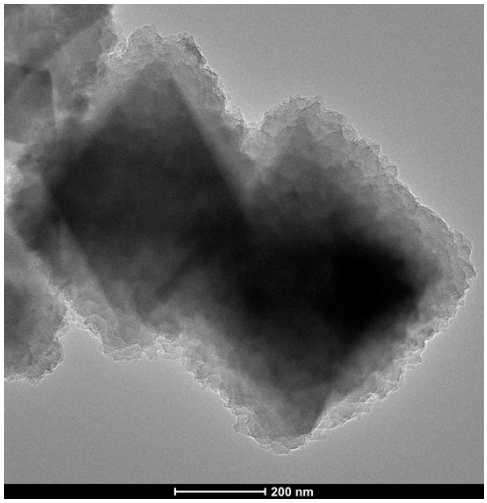

Fig S5. TEM images of UiO-66-NH_2@COF1

113 Table S1 Comparison of UiO-66-NH_2@COF1 with some other adsorbents recently reported

Materials	Target	qmax (mg g−1)	Temp. (K)	Equilibrium time (h)	Refs.
Fe_3O_4 @ ZTB-1	CR	458	308	2	[1]
ZIF-8@ZIF-67	CR	291.5	273	1	[2]
UiO-66-NH_2@COF1	CR	1503.7	308	4	This work
COF-CTTD	RB	684.9	308	2	[3]
MIL-68(Al)	RB	1111	308	1.5	[4]
UiO-66-NH_2@COF1	RB	2037.2	308	4	This work
ZIF-8@CS/PVA-ENF	MG	1000	308	3	[5]
KGM/ZIF-67	MG	2891.3	308	3.5	[6]
UiO-66-NH_2@COF1	MG	2228.6	308	4	This work

114

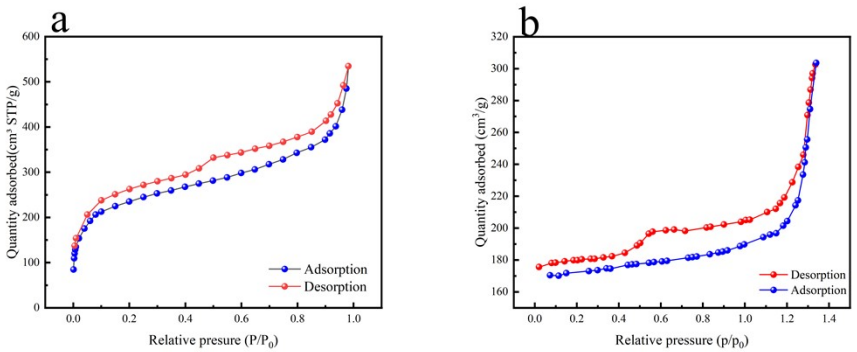

115

116 Fig S6 N_2 adsorption/desorption isotherms of UiO-66-NH_2@COF2 and UiO-66-NH_2@COF3.

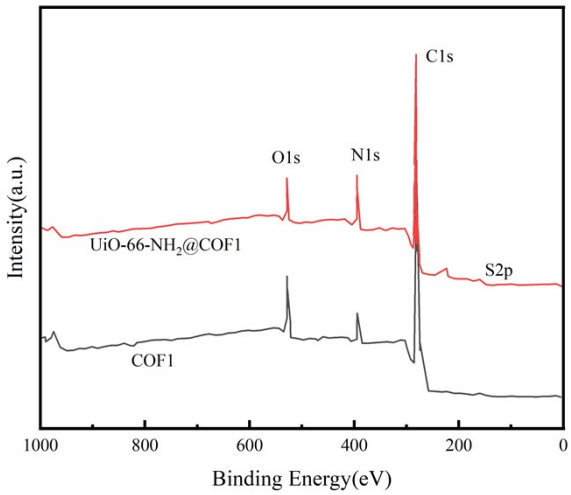

Fig S7 XPS spectrum of COF1 and UiO-66-NH_2@COF1

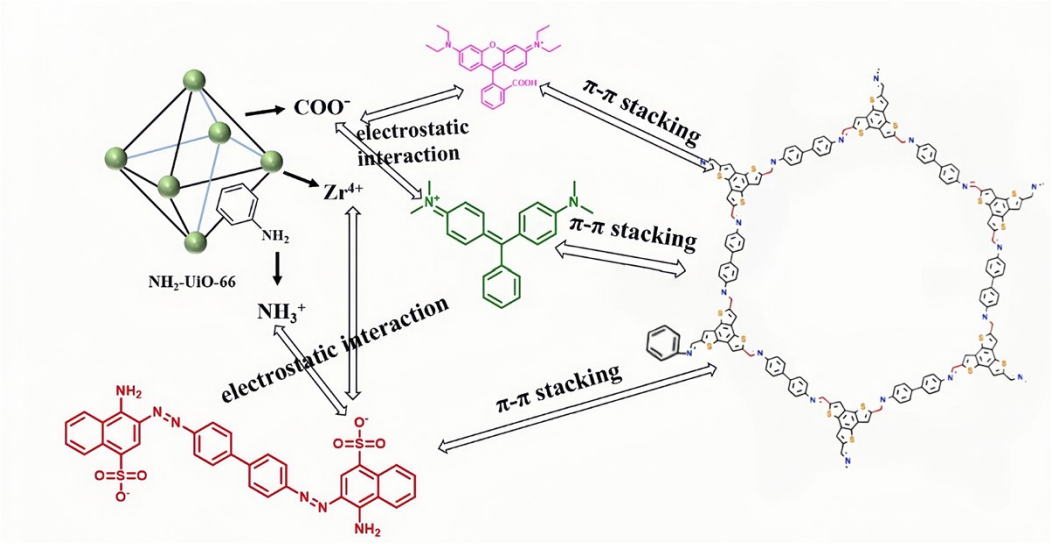

Fig S8 Possible mechanism of dyes adsorptions on UiO-66-NH_2@BTT-BZ

References

[1]. L. Han, F. Yuan, G. Sun, X. Gao and H. Zheng, *Dalton transactions (Cambridge, England : 2003),* 2019, **48,** 4650-4656.

[2]. C. Gu, W. Weng, C. Lu, P. Tan, Y. Jiang, Q. Zhang, X. Liu and L. Sun, *Chinese Journal of Chemical Engineering,* 2022, **42,** 42-48.

[3]. Q. Jiang, H. Huang, Y. Tang, Y. Zhang and C. Zhong, *Industrial & Engineering Chemistry Research,* 2018, **57,** 15114-15121.

[4]. M. Saghanejhad Tehrani and R. Zare-Dorabei, *RSC Advances,* 2016, **6,** 27416–27425.

[5]. B. L. Tran, H. Y. Chin, B. K. Chang and A. S. T. Chiang, *Microporous and Mesoporous Materials,* 2019, **277,** 149-153.

[6]. Z. Wu, X. Wang, J. Yao, S. Zhan, H. Li, J. Zhang and Z. Qiu, *Separation and Purification Technology,* 2021, **277,** 119474.